ADVANCED ENERGY MATERIALS
www.advenergymat.de

Flexible Film-Discharge-Switch Assisted Universal Power Management System for the Four Operation Modes of Triboelectric Nanogenerators

Wenjie Yan, Yuan Liu, Pengfei Chen, Leo N.Y. Cao, Jie An, Tao Jiang, Wei Tang, Baodong Chen, and Zhong Lin Wang**

Triboelectric nanogenerators (TENGs) are used to harvest high entropy energy. To optimize the energy harvesting, storage and effective utilization, a critical part is the power management system (PMS), which requires an ideal electrical switch as the key component. However, the current switch technologies cannot adapt and enhance the charging for the four operation modes of TENG simultaneously. Herein, a flexible film-discharge-switch (FDS), delivering an averaged charge-enhance factor over 100 under four operation modes of TENG, compared to directly charging a capacitor with conventional rectifier is reported. More specifically, the charge-enhancement factors of the FDS are 134.3, 64.7, 97.0, and 136.5 for the modes of contact-separation, lateral sliding, single-electrode, and freestanding triboelectric layer, respectively. Furthermore, the high flexibility, stability, simplicity, durability, and self-driven design of FDS endows the switch the possibility of versatile applications in the four modes of TENGs and flexible PMSs in wearable TENG applications. The successful demonstration in TENGs shows the great potential of the FDS in various fields such as micro-nano energy storage, distributed power supply, and self-powered systems.

1. Introduction

Triboelectric nanogenerator (TENG) as the most recent energy technology provides an ideal solution to harvest high entropy energy from nature and the human body, and to power billions of distributed electronics and sensor networks.[1,2] Compared with traditional energy generators, TENG has demonstrated great advantages in efficiency, flexibility, lightweight, environmentally friendly, and environmental adaptability.[3–5] As a brand-new invention by Z. L. Wang in 2012,[6] TENG takes a tremendous advancement in various aspects, such as triboelectric mechanism,[7–9] structure optimization,[10,11] material research,[12–14] application extension,[15–18] output power,[19,20] direct current (DC) TENG,[21–23] and power management system (PMS).[24]

However, TENG still has some problems to be addressed. For example, the energy-transfer efficiency from TENG to loads in real applications is not optimal. The reason is that TENG always mismatches with the impedance of load when directly powering electronics or storing electricity generated by the triboelectrification effect. Fortunately, as a bridge between TENG and electronics to reduce the mismatch and improve the energy-transfer efficiency,[24] PMS is invented. Consisting of a temporary storage capacitor (C_t), a switch, and a buck circuit,[25–29] PMS converts random energy from TENG into a steady DC power supply for driving electronics in high efficiency. For example, with and without a high-performance PMS in practical applications, the speed of energy storage in a capacitor can differ by two orders of magnitude.[30] Furthermore, the improvement is reported many times, such as quickly starting up and simultaneously driving multiple devices.[25,28,30,31]

The remarkable value of PMS has attracted a lot of attention and leads to various designs, following the same principle and similar topological structures but with different switch designs.[24,25,28] The study of switches, as the key component of PMS, becomes the main effort. In the early stage of switch development (from 2013), reported switches start the PMS field but are bounded together with and followed the movement of TENG, indicating the lowest adaptability in applications.[27,30,32–36] In the next development stage (from 2015), to investigate the principle of PMS, many active electronic switches are proposed and studied.[25,28,29] Using metal-oxide

W. Yan, Y. Liu, P. Chen, L. N.Y. Cao, J. An, T. Jiang, W. Tang, B. Chen, Z. L. Wang
CAS Center for Excellence in Nanoscience
Beijing Key Laboratory of Micro-nano Energy and Sensor
Beijing Institute of Nanoenergy and Nanosystems
Chinese Academy of Sciences
Beijing 101400, P. R. China
E-mail: chenbaodong@binn.cas.cn; zlwang@binn.cas.cn
W. Yan, Y. Liu, P. Chen, L. N.Y. Cao, J. An, T. Jiang, W. Tang, B. Chen, Z. L. Wang
School of Nanoscience and Technology
University of Chinese Academy of Sciences
Beijing 100049, P. R. China
Z. L. Wang
School of Materials Science and Engineering
Georgia Institute of Technology
Atlanta, GA 30332-0245, USA

The ORCID identification number(s) for the author(s) of this article can be found under https://doi.org/10.1002/aenm.202103677.

DOI: 10.1002/aenm.202103677

semiconductor field-effect transistors, this kind of switch is an energy expenditure device, resulting in low energy-transfer efficiency. In the following development stage (from 2020), combining a silicon-controlled rectifier and Zener diode, the self-driven switch is developed.[26,37] Although the self-driven switch is reported with good performance on the contact-separation (CS) mode of TENG, its efficiency is highly dependent on the electrical components on the market, especially when the voltage of TENG significantly exceeds the maximum acceptable range, indicating relatively low adaptability. In the recent development stage (from 2020), introducing the air breakdown principle in PMS field, two innovative studies about self-driven discharge switches are reported on the CS mode TENG, showing high energy-transfer efficiency and wide voltage range.[31,38] However, this kind of switches can still be improved on several aspects, such as light weighted, miniature, and flexible design, and precise and convenient control of the discharge distance. Besides, the DC TENG, invented by J. Wang's group, is a strategy to directly provide DC current without rectifier and provide high output power.[21–23] However, these reports are bounded and limited to their special designed TENGs.

In general, PMS switch technologies have achieved great progresses in improving the energy-transfer efficiency and self-driven design. However, no data reports any single switch can suit TENGs with all four operating modes, including CS, lateral sliding (LS), single-electrode (SE), and freestanding triboelectric layer (FTL) modes, simultaneously. In other words, the adaptability of PMS is an urgent challenge to be studied. In fact, the challenge is confirmed by existing researches, where around 70% of these reports focus on CS mode,[25,26,28–33,37–39] and the other reports focus on FTL mode,[25,27,34–36] namely, few studies focus on a versatile switch for all four operation modes.

Herein, inspired by the electrostatic discharge and shock, we report a flexible film-discharge-switch (FDS) for a universal PMS, which becomes compatible with all four operation modes of TENG, and the averaged charge-enhance factor maintains over 100, indicating 100 times faster than the traditional rectifier directly charging a capacitor. Detailed charge-enhance factors of CS, LS, SE, and FTL modes are 134.3, 64.7, 97.0, and 136.5, respectively. Furthermore, compared with reported switches, our FDS integrates many other advantages, including high energy-transfer efficiency close to 86.7%, minimalist design within 0.025 g, excellent durability survived from 1.25 million discharges, self-driven design, flexible and durable structure, and wide range of available voltage. To demonstrate the power of FDS on real-world applications, a PMS with an FDS is designed for distributed TENGs and manufactured, increasing the number of continuously lighted LED from 1 to 120, and the lighted screen time of an electronic hygrothermograph from only 8 s (per 9958 s charging time) to continuous working. In general, as a new technology of PMS switches, the flexible FDS has the potential to become a universal commercial electronic component customized for TENG applications, similar to diodes for modern circuits, indicating great applications in distributed power, energy storage, wearable applications, and Internet of Things.

2. Results and Discussion

As a common phenomenon in nature, air breakdown always happens in our life, such as huge lighting formed by the friction of clouds and tiny spark formed by the friction of cloths. Based on the same phenomenon, we invent a FDS that replaces the traditional switch of PMS. **Figure 1**a and Figure S1a (Supporting Information) exhibit the minimalist structure design of FDS, which only consists of a piece of insulation film, two pieces of conductive film, and two wires. The FDS is similar to parallel-plate capacitor, but with an additional insulation film, which parallelly separates two conductive edges. Since the breakdown voltage and the discharge distance are in positive linear correlation, the equal distance of conductive edges contributes a stable breakdown voltage of FDS (V_{FDS}), which can be precisely regulated and adjusted by replacing insulation films with different thicknesses (6 μm–1 mm). In Figure 1b, two discharge edges (copper foil tape), separated in parallel by the insulation film (PTFE layer), are used for auto discharge when the voltage between two conductive film surpasses the discharge voltage. Therefore, the FDS can stably work as a self-driven discharge switch in a PMS circuit.

Fabricating a FDS by hand is extremely simple. For example, we only need to prepare a few laboratory scraps shown in Figure S1b (Supporting Information). After combining them, trimming out discharge edges, and trimming off useless corners, we get a handmade FDS within several minutes. Figure 1c and Figure S2a (Supporting Information) provide a clear view of one tiny handmade FDS used in this paper. This FDS has a minimalist structure, a diameter less than 8 mm and a thickness of 80 μm (less than a piece of A4 paper), as demonstrated in Figure S2b,c (Supporting Information). Benefiting from the minimalist design, FDS is as light as feather with the weight less than 0.025 g, which almost adds no burden to TENG systems, shown in Figure S2d (Supporting Information). Therefore, FDS is user friendly to all laboratories with TENG experiments and promises a great potential for commercialization. More importantly, benefiting from the soft insulation film, the FDS becomes the first soft switch of PMS (Figure 1d), which will be the only choice for flexible PMS in wearable TENG applications.

Figure 1e exhibits a universal PMS circuit equipped with an FDS instead of the original switch. The FDS divides the working cycle of PMS into 2 steps: 1) During TENG output process, the off-state FDS forces charges to accumulate into C_t and increases the voltage of C_t (V_{C_t}) to the maximum value that TENG can provided (V_{max}). 2) After V_{C_t} reaching V_{FDS}, which is close to V_{max}, the FDS is on and all charges are instantly released from C_t to buck circuit in the form of a large current pulse, leading to a maximum charge transfer (Q_{max}). According to the formula of energy transfer,

$$E = \oint V\, dQ \tag{1}$$

the output energy is the area enclosed by V and Q in voltage–charge plot. Therefore, TENG reaches its maximum output $E_{max} = (1/2)V_{max}{}^{*}Q_{max}$ with the assistance of PMS and enables TENG to drive more electronic devices, shown in Figure S3a (Supporting Information). Without PMS, TENG is difficult to

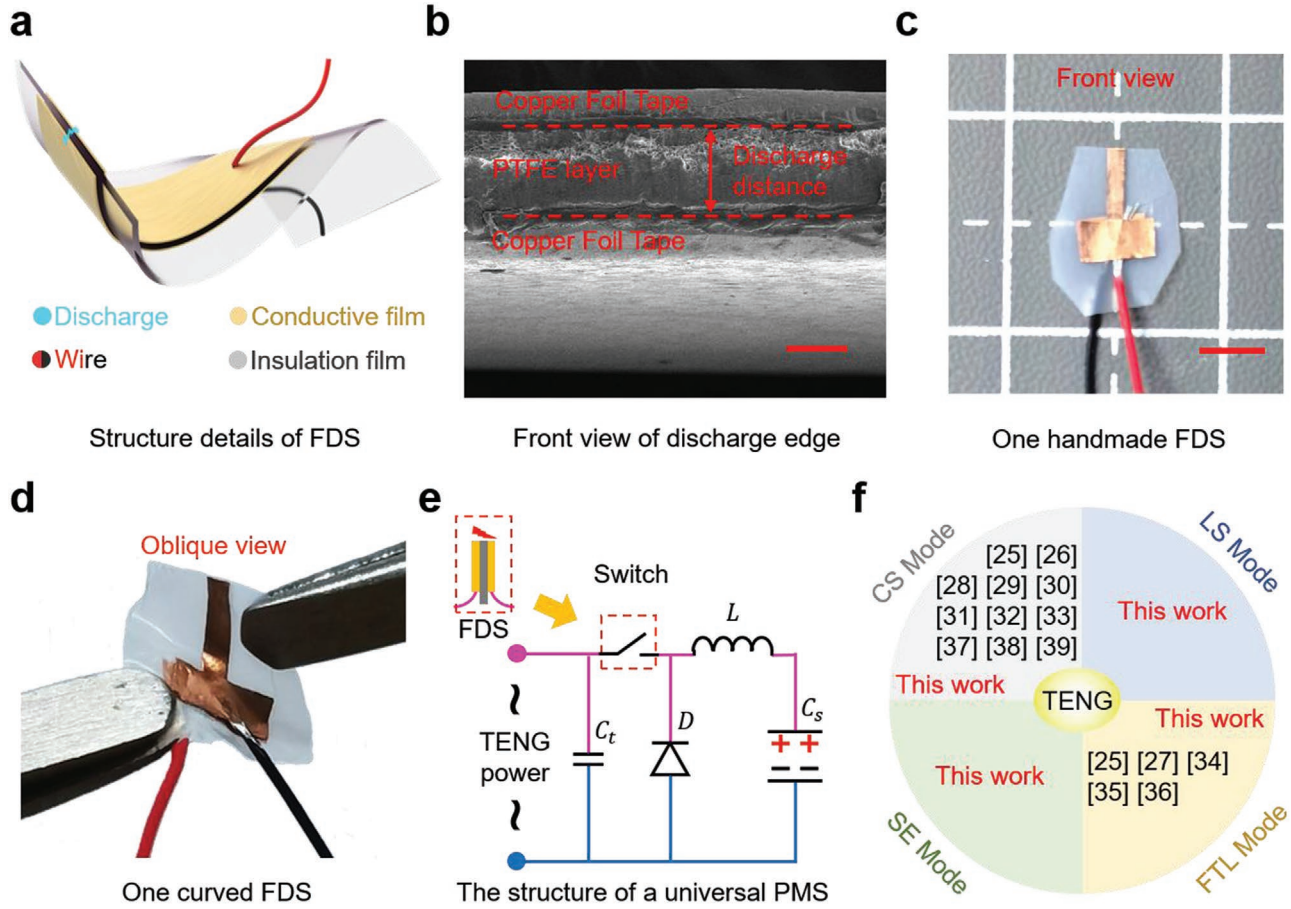

Figure 1. Structure design and working principle of the FDS. a) 3D view and composition of a flexible FDS. b) The SEM image of the front view of discharge edges shown a sandwich structure (scale bar: 50 µm). c) The front view of a handmade FDS (scale bar: 2 mm). d) The oblique view of a curved FDS. e) A universal PMS circuit with an FDS instead of a switch. f) The adaptability of this work compared with reported PMS strategies for the four operation modes of TENG.

simultaneously reach V_{max} and Q_{max} leading to low efficiency of output, shown in Figure S3b (Supporting Information). Most importantly, the FDS enables a universal PMS to function well for the four operation modes of TENG simultaneously (Figure 1f), indicating good adaptability, which benefits the PMS popularization. Detailed supporting data will be shown later.

To further characterize the FDS, we adopt the experimental schematics shown in **Figure 2**a, which can be divided into 3 parts, one CS mode TENG, half-rectifier, and a universal PMS with an FDS. As TENG runs, charges are periodically stored in C_t via the half-rectifier, and V_{C_t} gradually increases. When $V_{C_t} = V_{FDS}$, the FDS will be instantaneously on and charges stored are released to the buck circuit at the same time. Figure 2b is the only discharging frame of FDS in a discharging process captured by a high-speed camera at 10 000 fps. This image indicates the discharge duration is less than 0.1 ms. Other discharge images in different views are shown in Figure S4 and Video S1 and S2 (Supporting Information).

The shortest distance for air breakdown is the width between two parallel discharge edges, determined by the thickness of the insulation layer in the middle of FDS. In the following experiment, all data are collected in ambient room condition with humidity around 35–50%. The C_S (high-capacity capacitor) and L (inductance) are 1 mF and 5 mH, respectively. V_{FDS} as the most important parameter of FDS is determined by the thickness of insulation layer. Therefore, we connect FDSs to a high-voltage power source to check the relationship between V_{FDS} and the thickness of the insulation layer. Recorded in Figure 2c, the result exhibits that V_{FDS} increases as the thickness of the insulation layer increases, indicating V_{FDS} is easy to be precisely controlled in full voltage range via thickness.

Figure 2d is the voltage of C_s charged by TENG with and without PMS, which its FDS is checked by 9 different thicknesses. The C_t is 30 pF. To simplify the data presentation, we define the 0 µm thickness as direct charging through a half-rectifier. Based on this data, the time consumption of charging C_s from 0 to 2 V and the amount of charges stored in C_s of the very first discharge is summarized in Figure 2e. This data shows the time consumption rapidly reduced from 5168 s to below 100 s with an increased thickness of FDS, indicating a higher efficiency of energy-transfer with thicker FDS and higher V_{FDS}. The data also shows the amount of charge stored into C_s of the very first discharge gradually increased from 0.2 to 29 µC. Figure 2f exhibits the relationship between the voltage of C_t and the amount of charge stored in C_s. It shows that

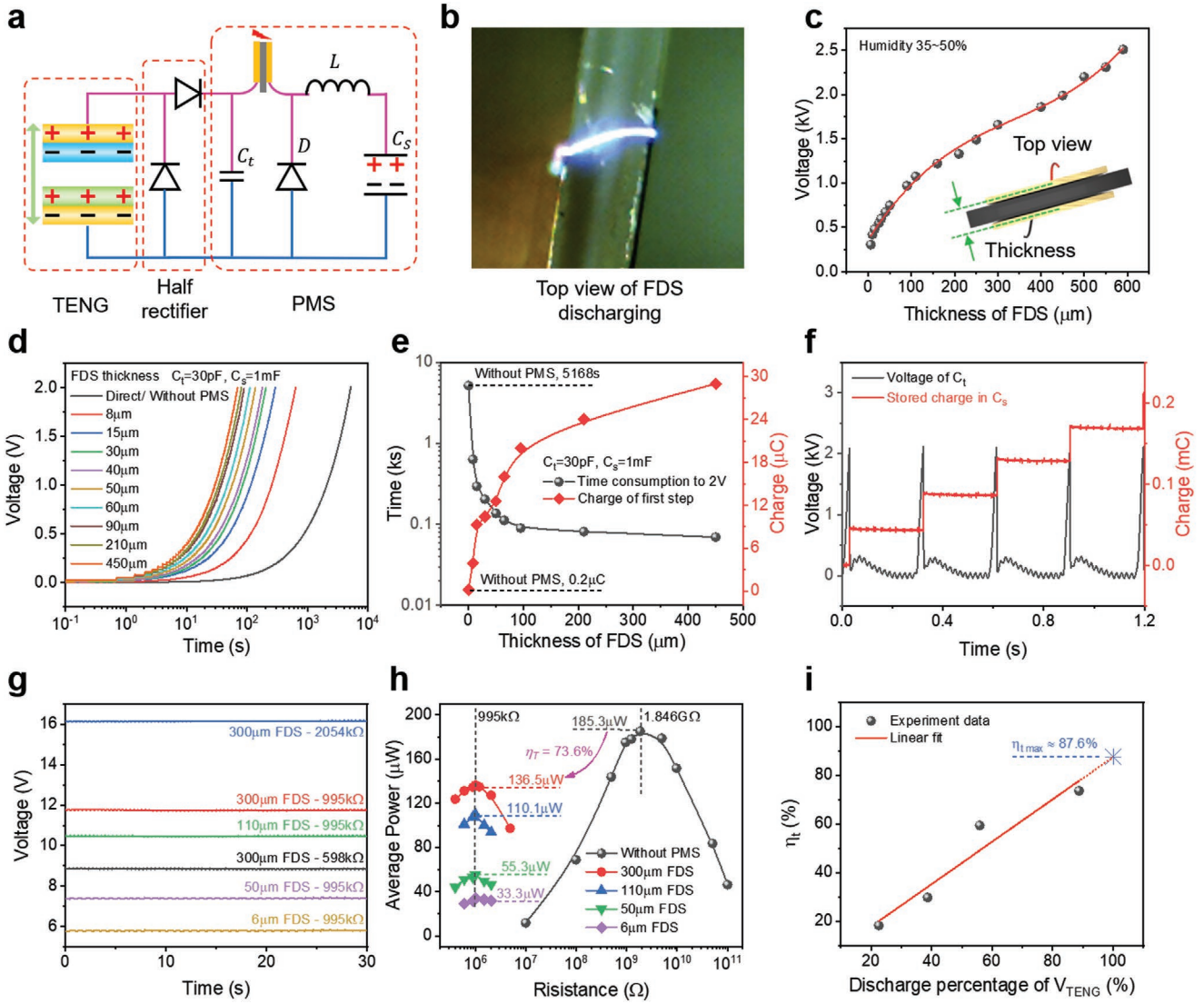

Figure 2. The basic performance of FDS in a common PMS circuit. a) Experiment schematic illustration divide into 3 parts, a CS mode TENG, a half-rectifier, and a PMS. b) A discharge frame captured by high-speed camera on 10 000 fps. c) The relationship between discharge voltage and the thickness of FDS. d) The voltage on C_s charging comparison by direct charging and PMS charging with multi-thickness FDS. e) The time consumption and the transformer charges of the first discharge pulse versus the thickness of FDS. f) The voltage and output charge of FDS when it is on/off as TENG running. g) Using PMS charging method, stable voltage curves of C_s with loading different resisters in parallel. h) Comparison of average output power with PMS and without represented by the black data and colorful data, respectively. i) The increment of η as a function of discharge percentage of V_{max} gradually close to 100%.

when V_{C_t} reaches ≈2050 V, FDS connects and releases energy instantly leading an abrupt decreasing of V_{C_t}, while ≈42.7 μC electrons are stored synchronously in C_s, finally leading to a stair steps curve of charge accumulation.

The energy-transfer efficiency η is the most important performance indicator of a PMS. It is calculated by the following equation:

$$\eta = \frac{P_1}{P_{max}} \times 100\% \quad (2)$$

where η reflects the ratio of maximum average output power from PMS (P_1) to the maximum average power transferred into PMS from TENG (P_{max}). P_{max} is obtained by measuring the current of resistors, which are directly connected behind the half-rectifier. P_1 is obtained by measuring a steady voltage of C_s, which is paralleled to resistors. 300, 110, 50, and 6 μm FDSs are checked and part of representative data for calculating P_1 is shown in Figure 2g. Then, the average output power between with and without PMS is shown in Figure 2h. It shows that the optimally matched resistance of TENG is 1.846 GΩ and its P_{max} is 185.3 μW. All optimally matched resistances of PMS with four different FDSs are 995 kΩ, reduced by 3 orders of magnitude, indicating that the influence of the thickness of FDS can be ignored. Figure 2h also reflects that the value of η increases synchronously as the thickness of FDS increases. The

maximum η we measured in the experiment is 73.6% under 300 µm-FDS. Essentially, as exhibited in Figure 2i, η and the percentage of V_{FDS} to V_{max} (V_{FDS}/V_{max}) are in positive linear correlation, indicating 87.6% should be the maximum value of η in this experiment.

Although η reflects the efficiency of energy-transfer of PMS, more attention is brought to the speed of charging a capacitor in the practical application of PMS, because the speed intuitively reflects the time efficiency of energy-transfer in a capacitor when comparing with traditional methods. Considering the practical application requirements, instrument accuracy, and calculation values, we define the charge-enhance factor (T_{Direct}/T_{PMS}) to represent the performance of PMS, where T is the time consumption of charging C_s from 0 to 2 V. Reasons of defining the factor are discussed in Figure S5 and Tables S1 and S2 (Supporting Information). For example, PMS reduces the time consumption from 100 s to 1 s for accumulating enough energy to start a loader. The charge-enhance factor in time efficiency of this PMS is as high as 100, indicating a great improvement of TENG performance from PMS. In fact, studying the charge-enhance factor provides a clear view of the performance of a PMS in TENG application. According to our knowledge, most reported studies about PMS are mainly based on CS mode TENG as discussed in Figure 2. However, as mentioned in previous section, no studies report one PMS working on all four operation modes of TENG simultaneously, indicating a relatively weak performance on the other 3 operation modes of TENG.

In **Figure 3**a, we systematically studied the energy-storage performance of a universal PMS equipped with FDS on four operation modes of TENG. In Figure 3a, the time consumption is recorded for four operation modes of TENG charging C_s from 0 to 2 V with varying C_t and the thickness of FDS. The results of CS mode TENG are exhibited in Figure S6b c (Supporting Information). According to these two figures about charging C_s, we observe the charging trend I, where the time consumption of charging firstly decreases and then increases as the C_t increasing. It indicates a most optimal value of C_t minimizing the time consumption of charging. To further analyze the charging trend, the minimum time consumption of each FDS and the corresponding most optimal C_t are summarized in Figure S6d (Supporting Information). According to this figure, we observe the charging trend II, where the minimum time consumption firstly decreases and then increases, but the most optimal C_t monotonically decreases to minimum.

The reason of the charging trends I and II is attributed to the mismatch between the cycles of the FDS discharging and TENG movement, leading to the FDS staying in a high-voltage state for a long time or the FDS discharging many times in one TENG cycle. Both negative effects contribute to the energy loss, such as leakage current, charge dissipation, and energy consumption of discharging. More analysis is shown in the discussion of Figure S6 (Supporting Information). Although it is obvious that two well-matched cycles of FDS discharging and TENG movement produce a good performance of PMS, it is difficult to meet the ideal working condition, because factors such as different types TENG and random frequency of mechanical energy cause the mismatch between FDS and TENG in practical applications. Therefore, to minimize the mismatch, C_t (Figure 2a) should be large when V_{FDS} is much lower than V_{max}, and it should be small when V_{FDS} is close to V_{max}. This conclusion is supported by Figure S10 (Supporting Information), that the best-matched C_t increased as increasing the amount of charge transferred from TENG.

Figure 3b shows four representative charging data of Figure S6d (Supporting Information) as well as the data of direct charging by the rectifier. The thicker FDS versus the smaller value of the most optimal C_t. Similar to Figure 3b, Figure 3c–e are the charging data obtained by the combination of other three operation modes of TENG in Figure 3a, and more detail data about C_t and the thickness of FDS are shown in Figures S7–S9 (Supporting Information), demonstrating the similar charging trend as discussed in Figure S6b–d (Supporting Information).

According to the previous experiments, we recorded the time consumption of four operation modes of TENG charging C_s from 0 to 2 V with PMS in Figure 3f, where each V_{FDS} is transferred into the percentage of V_{FDS}/V_{max}. The results show that the charge-enhance factor gradually increases as V_{FDS}/V_{max} approaches to 90%, and it decreases after V_{FDS}/V_{max} exceeds 90%. In general, it reaches its maximum value during 60–90% of V_{FDS}/V_{max}. More specifically, the charge-enhance factors of PMS are 134.3, 64.7, 97.0, and 136.5 in CS, LS, SE, and FTL modes, respectively, proving the PMS can work well in four operation modes of TENG. In addition, an average charge-enhance factor is 122.6 when V_{FDS} is 60–90% of V_{max} (excluding the LS mode). Since the experiment of LS mode should introduce a conductive slip ring, which will internally discharge when it exceeds a certain high voltage. For this reason, the data of LS mode is only measured the range of Figure 3f showed. In general, the FDS provides PMS an excellent universality for all four operation modes of TENG, removing a great obstacle for the commercialization of PMS technology.

In **Figure 4**a–c, as a necessary prerequisite for commercial application, an excellent durability of FDS has been proved by discharge tests. Figure 4a is the morphology of the discharge edge of an unused FDS, which has a relatively flat surface cut by scissors. Then, the FDS has withstood 1.25 million discharge tests, as shown in Figure 4b, which records the discharge data in the first 10 s of each hour of the first 8 h. After the durability test, the discharge voltage is maintained at around 2000 V, indicating that the FDS can be used as a long-life switch in a PMS circuit. However, 1.25 million discharge tests indeed change the morphology of discharge edge from flat to uneven, as comparing Figure 4a,c, indicating that discharge is a slow process of consuming the working life of FDS.

To demonstrate the performance of FDS, a PMS circuit and a direct charging circuit are used to compare the performance of a low-power TENG driving small electronic device and keep lighting LEDs. As shown in Figure 4d, one direct charging circuit and one PMS circuit are made on a breadboard, and their circuit corresponds to Figure 4e,f respectively. The energy is first transferred into C_s and then is used to driving a hygrothermograph in parallel with C_s as shown in Figure S11a,b and Video S3 (Supporting Information). The TENG takes 81 s to charge the C_s from 0 to 3 V through the PMS circuit, accompanied with a voltage reduction of C_s, the hygrothermograph is lighted as turning on the switch. In subsequent observations, as the energy input into C_s is greater than the energy consumption of

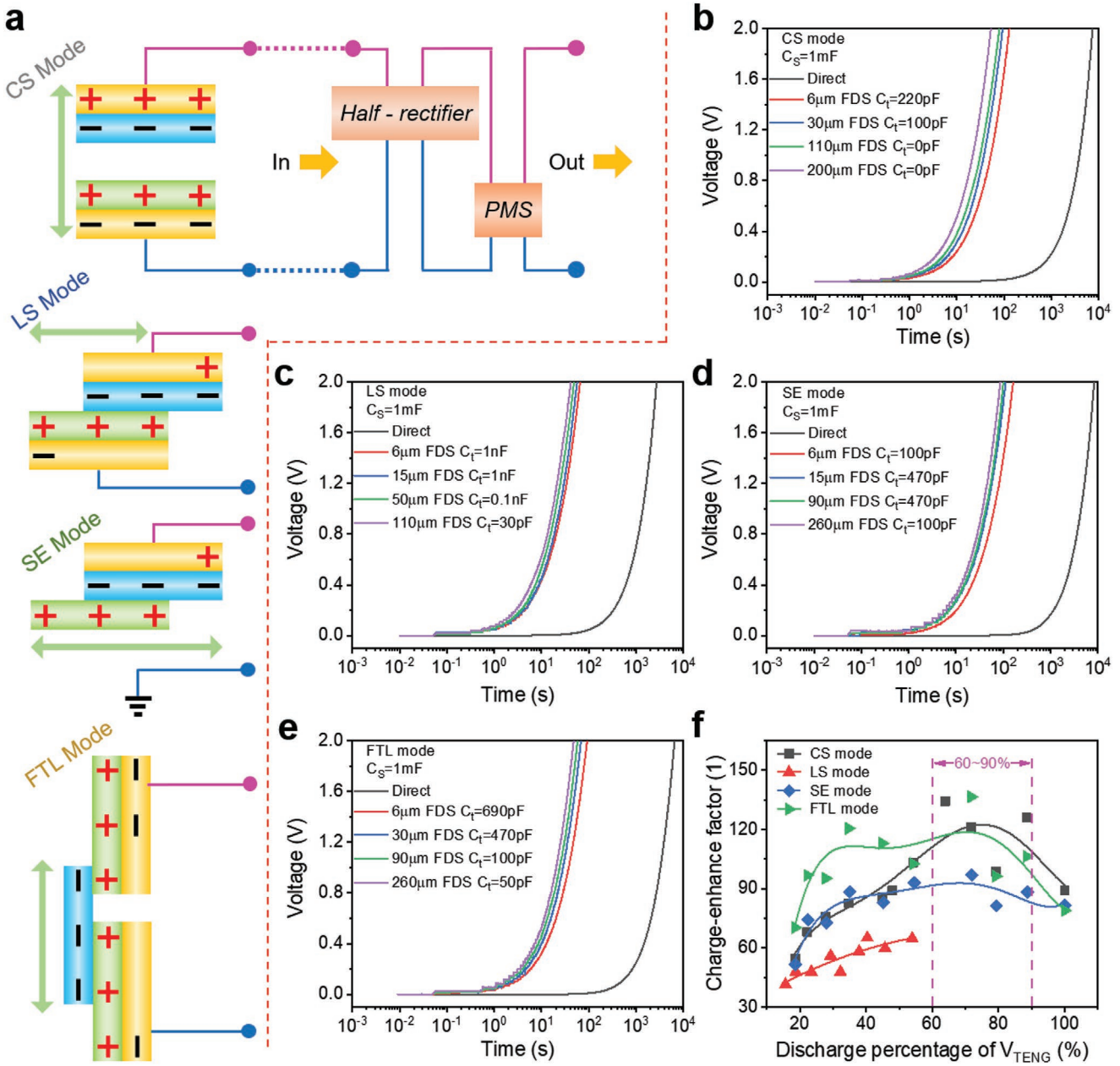

Figure 3. The adaptability of a universal PMS equipped with FDS for four operation modes of TENG. a) Schematic of experiment about energy-storage performance of PMS for four operation modes of TENG. b–e) The voltage-time curve of C_s using direct charging and PMS charging with 4 typical FDSs, corresponding to CS, LS, SE, and FTL modes of (a). f) The relationship of charge-enhance factor and discharge percentage of V_{max}.

hygrothermograph, the voltage of C_s increases slowly, and the device can keep working. In the comparative experiment, the same TENG takes 9958 s to charge the C_s from 0 to 3 V without PMS, with turning on the switch, the hygrothermograph is lighted for only 8 s with the voltage of C_s quickly dropped to 2.67 V (the lowest voltage to light the screen). Figure 4g reflects the variation of the voltage of hygrothermograph in the above experiment. It shows that the PMS reduces the boot-time from 9558 to 81 s, improving the time efficiency by 118 times, and enabling the device to work continuously, instead of a long charging time (a few hours) and a short working period (only a few seconds).

To further demonstrate the importance of FDS, we compared the difference of lighting LED when a TENG is used as the power source with and without PMS. This experiment is shown in Figure S11c,d and Video S4 (Supporting Information). The circuit is similar to Figure 4e,f, where the hygrothermograph is replaced by LEDs. Without PMS, the TENG only lights 1 LED at 1.921 V, as shown in Figure 4h. While, the PMS increases the number of LED from 1 to 120 under the same voltage, as shown in Figure 4j. Figure 4h reflects the variation of the voltage of LED on this experiment. It shows that the PMS improves the energy-transfer efficiency by 120 times. These two experiments show that the PMS can

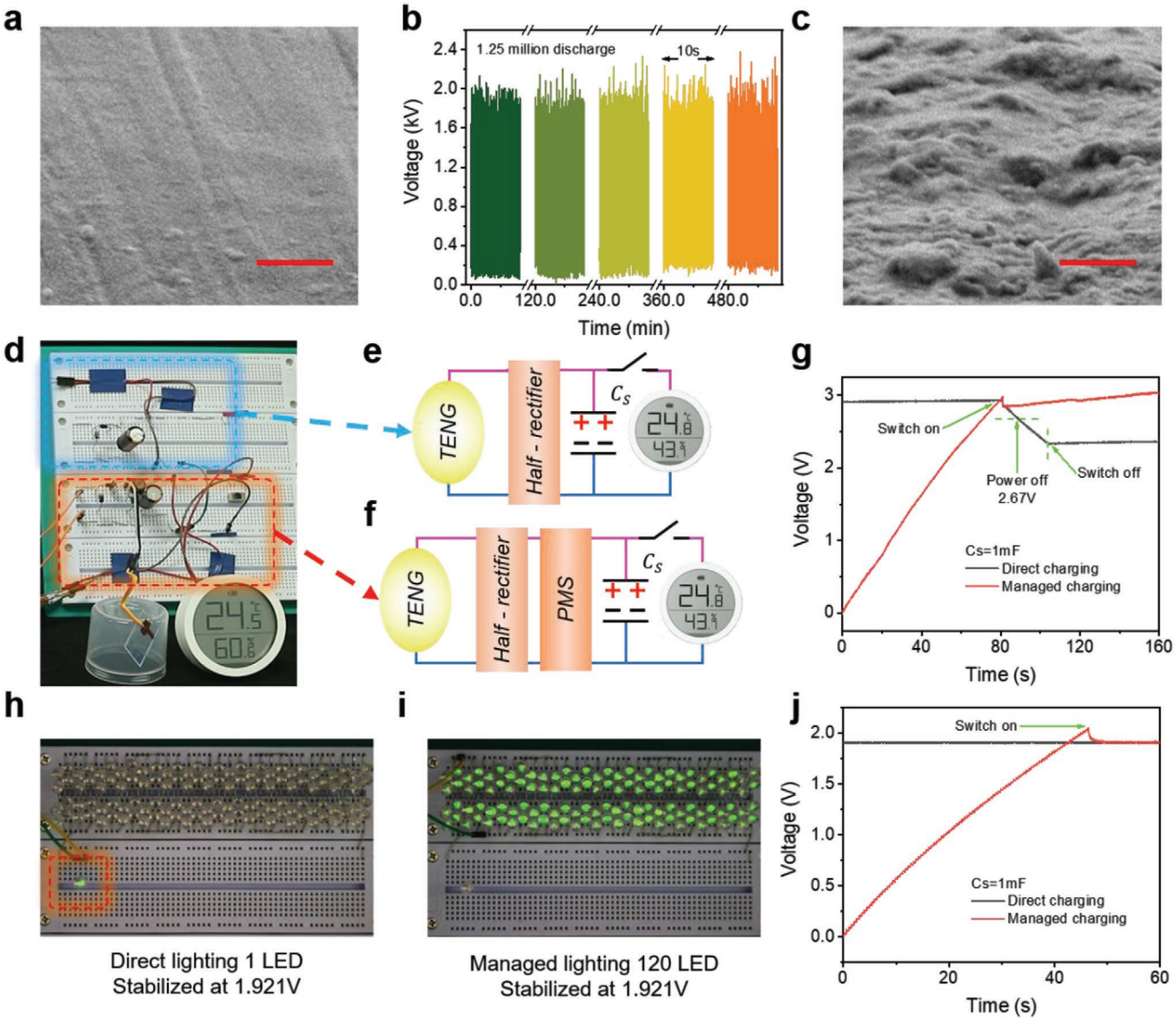

Figure 4. Durability and practicability of FDS. a) The morphology of discharge edge of a new FDS (scale bar: 5 µm). b) Data fragment of 1.25 million discharge in the durability test. c) The morphology of discharge edge after 1.25 million discharge test (scale bar: 5 µm). d) Direct charging circuit and PMS circuit in application experiment. e) The diagram of direct charging circuit with a hygrothermograph parallel connected to C_s. f) The diagram of PMS circuit with a hygrothermograph parallel connected to C_s. g) The voltage of hygrothermograph driven by TENG with/without PMS. h) TENG lights up 1 LED at 1.921 V by direct charging circuit. i) TENG lights up 120 LEDs at 1.921 V by PMS circuit. j) The voltage of C_s in (h) and (i) when lighting LED at 1.921 V.

significantly improve the efficiency of energy extraction from TENG.

The previous experiment exhibits the FDS, as a new flexible PMS switch technology suit for all four operation modes of TENG, can significantly improve the efficiency of energy extraction from TENG to bulk capacitor and electron expenditure devices. All designed by the breakdown air principle, we noted other two recent reports about PMS discharging switch: the plasma switch and the spark switch.[31,38] The plasma switch is suitable for low voltage TENG (≈500 V) with MEMS method to fabricate a micrometer-level discharge distance;[38] the spark switch is suitable for high voltage TENG (≈7500 V) with two large, heavy, and rigid metal parallel plates to form a millimeter-level discharge distance.[31] However, there is a gap between the working voltage range from several hundred to several thousand, which is the working voltage of majority reported TENGs. Benefited from the minimalist structure design, our FDS is easy and precise to fabricate a discharge distance from several micrometers to several millimeters, which produces a wider range of working voltage (350–3000 V) and is more compatible with the most reported TENGs. Besides, FDS also integrates many advantages including flexibility, stability, simplicity, durability, and self-driven design. The flexibility feature endows the FDS to be the first reported soft PMS switch, which may play a critical component of wearable TENG applications. These merits enable FDS almost suitable for all TENG

researches in all laboratories and promise a high potential for commercial application.

3. Conclusion

We have presented a flexible FDS used in a universal PMS, which shows good adaptability and flexibility to apply on the four operation modes of TENGs for the first time, and the averaged charge-enhance factor maintains over 100, namely, the PMS is about 100 times faster than traditional charging method. In order to improve the charge-enhance factor, we systematically optimized the FDS and C_t in PMS circuit. Charge-enhance factors of CS, LS, SE, and FTL modes reach 134.3, 64.7, 97.0, and 136.5, respectively. Furthermore, the practical applicability of developed FDS is successfully demonstrated with excellent properties in energy storage and power supply for small electronics, such as increasing the number of LED continuously lighted from 1 to 120, and improving the working time of an electronic hygrothermograph from 8 s (per 9958 s charging time) to work continuously, as well as 1.25 million-cycle overwhelming durability test. The various advantages of FDS, such as high flexibility, stability, simplicity, durability, and self-driven design, brings a great opportunity in energy storage of all four operation modes of TENG and in flexible PMS in wearable TENG applications.

4. Experimental Section

Fabrication of FDS: Referring to Figure S1b (Supporting Information), one piece of copper foil tape was cut into two 8×1 mm^2 scraps and two 3×2 mm^2 scraps. The two 8×1 mm^2 scraps were attached on both sides of one piece of insulation film and their outlines overlap. Two wires were fixed on the end of the two 8×1 mm^2 scraps using the two 3×2 mm^2 scraps. After trimming discharge edges out and trimming off corners of the insulation film, a new FDS was fabricated.

Fabrication of CS Mode TENG: Two pieces of 3 mm thickness acrylic board were cut into 10×15 cm^2 substrates by laser cutter (PLS6.75). Two pieces of 3 mm thickness foam were cut into 8×13 cm^2 substrates by laser cutter and adhered to the center of two acrylic substrates. An 8×13 cm^2 piece of copper film and an 8×13 cm^2 piece of A4 paper were pasted together as one contact-separation electrode. An 8×13 cm^2 piece of copper film and an 8×13 cm^2 piece of 100 µm thickness PVC film were pasted together as the other contact-separation layer. Two contact-separation electrodes were pasted to the surface of foam. Finally, two wires were drawn from two copper layers as output ends of TENG.

Fabrication of LS Mode TENG: This structure contained a rotating disk and a stator disk. Two pieces of 3 mm thickness acrylic board were cut into $\pi(\frac{13}{2})^2$ cm^2 disks by laser cutter. Two pieces of foam in the same size were pasted on one surface of acrylic disks. On foam surface, each acrylic disk contained 8 fan-shaped area, the outer diameter and inner diameter of each fan-shaped were 13 cm and 1.3 cm, and the distance of each fan-shaped was 5 mm. Four pieces of copper film were pasted to each acrylic substrate at intervals. One of the disks was covered by a piece of 100 µm thickness PVC film on the surface contained copper film. The PVC surface on one acrylic disk and the copper surface on the other acrylic disk were the lateral sliding layer. On each acrylic disk, all copper films were connected and drawn a wire out as the output end of TENG. Finally, the wire on rotating disk was connected to a conductive slip ring.

Fabrication of SE Mode TENG: This structure contained a rotating disk and a stator disk. Two pieces of 3 mm thickness acrylic board were cut into $\pi(\frac{13}{2})^2$ cm^2 disks by laser cutter. Each acrylic disk contained 8 fan-shaped area, the outer diameter and inner diameter of each fan-shaped were 13 and 1.3 cm, and the distance of each fan-shaped was 5 mm. For the rotating disk, 4 pieces of rabbit furs were pasted to 4 pieces of 8 fan-shaped area at intervals. For the stator disk, 8 pieces of copper film were pasted to 8 fan-shaped area, and a $\pi(\frac{13}{2})^2$ cm^2 piece of 50 µm thickness PTFE film was covered on the surface of copper layer. The PTFE surface on the stator disk and the rabbit furs on the rotating disk were the tribology layer. For the stator disk, the 4 electrodes at intervals of the 8 electrodes were connected to each other, then two wires as the output end of this TENG were drawn. For SE mode TENG, only one of the two wires was connected to circuits.

Fabrication of FTL Mode TENG: Similar to the fabrication of the SE mode TENG, two wires were connected to circuits.

Measurements: The CS mode TENG was implemented by a linear motor (TSMV120-1S), and the other three mode TENGs were implemented by a rotational motor (60ST-M01930). The transferred charge, the output current, and the voltage of capacitor were measured by Keithley 6514. The breakdown voltage of FDS in Figure 2c was measured by a high-voltage source (Keithley 2290-10). The discharge voltage as the numerator to calculate the discharge percentage of V_{TENG} was TREK 347. The surface morphology of the FDS in Figure 4a,c and Figure S2d (Supporting Information) were observed using a Nova NanoSEM 450 field emission scanning electron microscopy.

Supporting Information

Supporting Information is available from the Wiley Online Library or from the author.

Acknowledgements

W.Y. and Y.L. contributed equally to this work. The authors acknowledge the support from Beijing Natural Science Foundation (Grant No. 2192062), supported by National Natural Science Foundation of China (Grant No. 51502147, 51702018, and 11704032). The research was sponsored by the National Key R & D Project from Minister of Science and Technology (2016YFA0202704), China Postdoctoral Science Foundation (No. 2021M703174), and the Beijing Municipal Science and Technology Commission (Z181100003818016 and Y3993113DF).

Conflict of Interest

The authors declare no conflict of interest.

Data Availability Statement

The data that support the findings of this study are available from the corresponding author upon reasonable request.

Keywords

triboelectric nanogenerators, power management system, film-discharge-switches, charge-enhancement

Received: November 23, 2021
Revised: December 27, 2021
Published online:

[1] C. S. Wu, A. C. Wang, W. B. Ding, H. Y. Guo, Z. L. Wang, *Adv. Energy Mater.* **2019**, *9*, 1802906.
[2] Z. L. Wang, *Rep. Prog. Phys.* **2021**, *84*, 096502.
[3] Z. L. Wang, J. Chen, L. Lin, *Energy Environ. Sci.* **2015**, *8*, 2250.
[4] Y. Zi, S. Niu, J. Wang, Z. Wen, W. Tang, Z. L. Wang, *Nat. Commun.* **2015**, *6*, 8376.
[5] R. K. Gupta, Q. Shi, L. Dhakar, T. Wang, C. H. Heng, C. Lee, *Sci. Rep.* **2017**, *7*, 41396.
[6] F. R. Fan, Z. Q. Tian, Z. L. Wang, *Nano Energy* **2012**, *1*, 328.
[7] M. Willatzen, L. L. Y. C. Voon, Z. L. Wang, *Adv. Funct. Mater.* **2020**, *30*, 1910461.
[8] L. C. Lew Yan Voon, J. E. Hasbun, M. Willatzen, Z. L. Wang, *EcoMat* **2021**, *3*, e12086.
[9] J. J. Shao, T. Jiang, Z. L. Wang, *Sci. China: Technol. Sci.* **2020**, *63*, 1087.
[10] P. Lu, H. Pang, J. Ren, Y. Feng, J. An, X. Liang, T. Jiang, Z. L. Wang, *Adv. Mater. Technol.* **2021**, *6*, 2100496.
[11] C. G. Zhang, L. X. He, L. L. Zhou, O. Yang, W. Yuan, X. L. Wei, Y. B. Liu, L. Lu, J. Wang, Z. L. Wang, *Joule* **2021**, *5*, 1613.
[12] Z. Zhao, L. Zhou, S. Li, D. Liu, Y. Li, Y. Gao, Y. Liu, Y. Dai, J. Wang, Z. L. Wang, *Nat. Commun.* **2021**, *12*, 4686.
[13] H. Zou, Y. Zhang, L. Guo, P. Wang, X. He, G. Dai, H. Zheng, C. Chen, A. C. Wang, C. Xu, Z. L. Wang, *Nat. Commun.* **2019**, *10*, 1427.
[14] B. Y. Lee, D. H. Kim, J. Park, K. I. Park, K. J. Lee, C. K. Jeong, *Sci. Technol. Adv. Mater.* **2019**, *20*, 758.
[15] A. Ahmed, I. Hassan, M. F. El-Kady, A. Radhi, C. K. Jeong, P. R. Selvaganapathy, J. Zu, S. Ren, Q. Wang, R. B. Kaner, *Adv. Sci.* **2019**, *6*, 1802230.
[16] Q. Gao, T. Cheng, Z. L. Wang, *Extreme Mech. Lett.* **2021**, *42*, 101100.
[17] H. Askari, A. Khajepour, M. B. Khamesee, Z. L. Wang, *Nano Energy* **2019**, *66*, 104103.
[18] J. H. Han, K. M. Bae, S. K. Hong, H. Park, J. H. Kwak, H. S. Wang, D. J. Joe, J. H. Park, Y. H. Jung, S. Hur, C. D. Yoo, K. J. Lee, *Nano Energy* **2018**, *53*, 658.
[19] P. F. Chen, J. An, R. W. Cheng, S. Shu, A. Berbille, T. Jiang, Z. L. Wang, *Energy Environ. Sci.* **2021**, *14*, 4523.
[20] Z. Zhao, Y. Dai, D. Liu, L. Zhou, S. Li, Z. L. Wang, J. Wang, *Nat. Commun.* **2020**, *11*, 6186.
[21] S. Chen, D. Liu, L. Zhou, S. Li, Z. Zhao, S. Cui, Y. Gao, Y. Li, Z. L. Wang, J. Wang, *Adv. Mater. Technol.* **2021**, *6*, 2100195.
[22] D. Liu, L. Zhou, Z. L. Wang, J. Wang, *iScience* **2021**, *24*, 102018.
[23] Y. K. Gao, D. Liu, L. L. Zhou, S. X. Li, Z. H. Zhao, X. Yin, S. Y. Chen, Z. L. Wang, J. Wang, *Nano Energy* **2021**, *85*, 106014.
[24] X. L. Cheng, W. Tang, Y. Song, H. T. Chen, H. X. Zhang, Z. L. Wang, *Nano Energy* **2019**, *61*, 517.
[25] X. L. Cheng, L. M. Miao, Y. Song, Z. M. Su, H. T. Chen, X. X. Chen, J. X. Zhang, H. X. Zhang, *Nano Energy* **2017**, *38*, 448.
[26] W. Harmon, H. Y. Guo, D. Bamgboje, T. S. Hu, Z. L. Wang, *Nano Energy* **2021**, *85*, 105956.
[27] H. F. Qin, G. Q. Gu, W. Y. Shang, H. C. Luo, W. H. Zhang, P. Cui, B. Zhang, J. M. Guo, G. Cheng, Z. L. Du, *Nano Energy* **2020**, *68*, 104372.
[28] F. B. Xi, Y. K. Pang, W. Li, T. Jiang, L. M. Zhang, T. Guo, G. X. Liu, C. Zhang, Z. L. Wang, *Nano Energy* **2017**, *37*, 168.
[29] S. Niu, X. Wang, F. Yi, Y. S. Zhou, Z. L. Wang, *Nat. Commun.* **2015**, *6*, 8975.
[30] W. Liu, Z. Wang, G. Wang, Q. Zeng, W. He, L. Liu, X. Wang, Y. Xi, H. Guo, C. Hu, Z. L. Wang, *Nat. Commun.* **2020**, *11*, 1883.
[31] Z. Wang, W. L. Liu, W. C. He, H. Y. Guo, L. Long, Y. Xi, X. Wang, A. P. Liu, C. G. Hu, *Joule* **2021**, *5*, 441.
[32] G. Cheng, Z. H. Lin, L. Lin, Z. L. Du, Z. L. Wang, *ACS Nano* **2013**, *7*, 7383.
[33] G. Cheng, Z. H. Lin, Z. L. Du, Z. L. Wang, *Adv. Funct. Mater.* **2014**, *24*, 2892.
[34] H. F. Qin, G. Cheng, Y. L. Zi, G. Q. Gu, B. Zhang, W. Y. Shang, F. Yang, J. J. Yang, Z. L. Du, Z. L. Wang, *Adv. Funct. Mater.* **2018**, *28*, 1805216.
[35] W. Y. Shang, G. Q. Gu, W. H. Zhang, H. C. Luo, T. Y. Wang, B. Zhang, J. M. Guo, P. Cui, F. Yang, G. Cheng, Z. L. Du, *Nano Energy* **2021**, *82*, 105725.
[36] Y. L. Zi, H. Y. Guo, J. Wang, Z. Wen, S. M. Li, C. G. Hu, Z. L. Wang, *Nano Energy* **2017**, *31*, 302.
[37] W. Harmon, D. Bamgboje, H. Y. Guo, T. S. Hu, Z. L. Wang, *Nano Energy* **2020**, *71*, 104642.
[38] H. Zhang, F. Marty, X. Xia, Y. Zi, T. Bourouina, D. Galayko, P. Basset, *Nat. Commun.* **2020**, *11*, 3221.
[39] X. Wang, S. Niu, F. Yi, Y. Yin, C. Hao, K. Dai, Y. Zhang, Z. You, Z. L. Wang, *ACS Nano* **2017**, *11*, 1728.